Noncompliant Capacity Ratio for Systems With an Arbitrary Number of Polarization Hinges

Jinglai Li, Gino Biondini, Herwig Kogelnik, *Life Fellow, IEEE, Fellow, OSA*, and Peter J. Winzer, *Senior Member, IEEE, Member, OSA*

***Abstract*—We study the statistics of transmission impairments due to polarization-mode dispersion in systems characterized by the hinge model. In particular, we validate the use of a computationally efficient expression for the probability density function (PDF) of the differential group delay (DGD) of systems with an arbitrary number of hinges. We then combine this expression for the PDF of the DGD with the outage map approach to compute outage probabilities and noncompliant capacity ratios for transmission links with varying numbers of sections (from 4 up to 20), each for several values of mean DGD and different system parameters.**

***Index Terms*—Hinge model, noncompliant capacity ratio, optical fiber communications, outage probability, polarization mode dispersion.**

I. Introduction

THE proper specification of outage probabilities due to polarization-mode dispersion (PMD) in optical fiber transmission systems has been well studied under the assumption of Maxwellian statistics for the differential group delay (DGD) [1], [2]. Recent field measurements on deployed optical fiber plants, however, have shown that this assumption is often violated. In its place, a hinge model [3]–[6] of PMD has been proposed to characterize the behavior of the fiber transmission system. The hinge model assumes that the transmission link consists of several sections of long fiber, well protected from environmental changes, that are stable in their PMD characteristics over long periods of time (months). These stable sections are connected by "hinges" which act as rapidly varying polarization transformers. The hinges could be amplifier sites, servicing huts with variations in temperature, fiber cables exposed to mechanical vibrations on, e.g., railroad bridges, etc. The number of such sections in a typical transmission link is estimated to be between five and ten or more [3].

Two conditions set the limits of validity for the hinge model. One is the time scale over which the DGD of each section remains constant. The other is the time scale over which the hinges provide uniform coverage of the Poincaré sphere. The hinge model retains the traditional assumption that the DGD of each section, though frozen in time, still follows Maxwellian statistics as a function of wavelength, corresponding to the mean DGD of that section. Thus, each section has a statistically different DGD value for each wavelength band, as determined by the section's bandwidth of the principal state [2]. The outage characteristics of different wavelength bands are, therefore, statistically independent. Note that, in this context, a wavelength band may contain one or more wavelength-division-multiplexed (WDM) channels. It is, therefore, necessary to speak of wavelength *bands* rather than of WDM channels.

A specific feature of the hinge model is that a certain fraction of bands are found to violate any specified outage criterion [7], which leads to a paradigm shift in the way PMD system outage must be dealt with. In particular, a quantity called the noncompliant capacity ratio (NCR) was introduced in [7] as the fraction of WDM channels that do not comply with a given outage specification. Note that, in order for the NCR to be a useful quantity, the number of statistically independent WDM channels must be large. In the traditional model of PMD, all wavelength bands are statistically identical, and, therefore, they are either all compliant $(\mathrm{NCR} = 0)$ or all noncompliant $(\mathrm{NCR} = 1)$ with a given outage specification. This is not the case, however, if PMD is described by the hinge model.

In the traditional model of PMD, the value of the total DGD is assumed to follow a Maxwellian distribution over time, and the angular distribution of the PMD vector is taken to be uniform. For the hinge model, the angular distribution is still taken to be uniform, but the probability density function (PDF) of the DGD equals that of an emulator with fixed DGD elements connected by polarization transformers varying over time like the hinges. Analytic expressions for the PDF of the DGD in both the traditional and the hinge model of PMD are available [8], [9], and the expression for the PDF due to Antonelli and Mecozzi [9] was used in [7] for the development of precise outage data of links with six sections for the hinge model, using the outage map approach [10], [11]. System designers, however, need accurate data for transmission links with larger numbers of sections (up to about 20), in order to assess system outage and to develop strategies for PMD compensation. They are also interested in the sensitivity of the outages to changes in the number of hinges (which is sometimes uncertain). The approach used in [7] encountered computational difficulties when the number of hinges increased. Here, we, therefore, explore more efficient methods for the computation of the PDF of the DGD for systems with an arbitrary number of sections. We then use these methods to perform simulations in order to compute the system outage probability and NCR for links with varying numbers of sections between four and 20.

Manuscript received October 17, 2007; revised January 29, 2008. Published August 29, 2008 (projected). This work was supported by the National Science Foundation under Grant DMS-0506101.

J. Li and G. Biondini are with the Department of Mathematics, State University of New York at Buffalo, Buffalo, NY 14260 USA (e-mail: biondini@buffalo.edu).

H. Kogelnik and P. J. Winzer are with Bell Labs, Alcatel-Lucent, Holmdel, NJ 07733 USA.

Color versions of one or more of the figures in this paper are available online at http://ieeexplore.ieee.org.

Digital Object Identifier 10.1109/JLT.2008.920133

II. PDF of the DGD in the Hinge Model

As mentioned earlier, the hinge model of PMD characterizes a transmission link as a finite sequence of long fiber sections with fixed properties, connected by dynamically varying "hinges." Recall that, at each frequency, the growth of polarization-dependent effects for a concatenation of a finite number of sections is governed by the PMD concatenation equations (e.g., see [12]). In particular, for first-order PMD, the concatenation equation is

$$\vec{\tau}^{(n+1)} = \mathsf{R}_{n+1}\mathsf{H}_n\,\vec{\tau}^{(n)} + \Delta\vec{\tau}_{n+1} \tag{1}$$

where $\vec{\tau}^{(n)}$ is the total PMD vector after the nth section and before the nth hinge, the fixed vector $\Delta\vec{\tau}_n$ is the PMD vector of the nth section, R_n is the rotation matrix of the nth section and H_n the rotation matrix originating from the nth hinge. As in [6] and [7], we assume that the DGD $\Delta\tau_n = |\Delta\vec{\tau}_n|$ of each section is constant in time and that it follows a Maxwellian distribution in wavelength. Also, for simplicity, in all the numerical simulations that will be discussed in Section IV, we assume that the DGD distributions of each section have identical mean DGD. Note, however, that neither the hinge model itself nor the computational methods we describe are restricted to such a limitation.

Under the above assumptions, the only temporal variations in (1) arise from the hinge rotation matrix H_n. As customary, we assume that the hinges act as polarization controllers which scatter the previous PMD vector evenly across the Poincaré sphere. With this assumption, (1) becomes

$$\vec{\tau}^{(n+1)} = \mathsf{S}_{n+1}\left(\vec{\tau}^{(n)} + \Delta\vec{\tau}_{n+1}\right) \tag{2}$$

where $\mathsf{S}_{n+1} = \mathsf{R}_{n+1}\mathsf{H}_n$ and where $\Delta\vec{\tau}'_{n+1} = \mathsf{S}_{n+1}^{-1}\Delta\vec{\tau}'_{n+1}$ is now randomly and uniformly distributed on the Poincaré sphere. Then, if one is only interested in the total DGD $\tau_N = |\vec{\tau}_N|$, the matrix S_{n+1} is unessential, and the dynamics of first-order PMD becomes equivalent to that of a 3-D random walk, the statistics of which have been well studied in literature. We provide here sufficient detail for its use by others. In particular, a closed-form expression for the PDF of the DGD was obtained in [9]

$$p_{\mathrm{DGD}}(\tau;\mathbf{z}) = C_N\tau\sum_{k=1}^{2^N}(-1)^{\sigma_k}(T_k-\tau)^{N-2}\theta(T_k-\tau) \tag{3}$$

with $T_k = \pm\Delta\tau_1 \pm \Delta\tau_2 \pm \cdots \pm \Delta\tau_N$, where $\theta(\cdot)$ is Heaviside's unit step function, σ_k is the number of minus signs in T_k and $C_N = 1/[2^{N-1}(N-2)!\Delta\tau_1\cdots\Delta\tau_N]$. Here and below, $\mathbf{z} = (\Delta\tau_1,\ldots,\Delta\tau_N)$ is the N-component vector that collects the individual DGD of all sections. The evaluation of (3) requires a sum of 2^N terms. Therefore, its computational cost grows exponentially with N, and its use becomes prohibitive already for moderate values of N. Fortunately, the PDF of the DGD can also be obtained from the sum of an infinite Fourier series [8]

$$p_{\mathrm{DGD}}(\tau;\mathbf{z}) = 2\pi\frac{\tau}{\tau_{\max}^2}\sum_{m=1}^{\infty}c_m\sin\left(\frac{m\pi\tau}{\tau_{\max}}\right) \tag{4a}$$

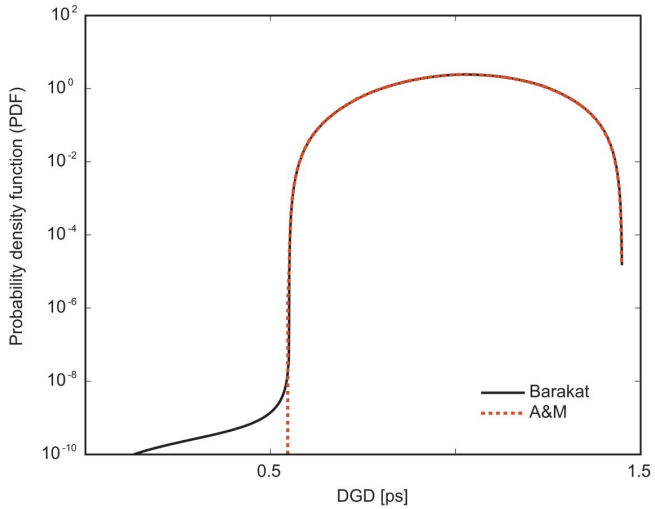

Fig. 1. PDF of the DGD on a logarithmic scale, for a system consisting of four sections, with individual DGDs of 0.1, 0.15, 0.2, and 1 ps, respectively. The solid line is the PDF computed using Barakat's formula with 2^{11} Fourier modes; the dashed line is obtained from (3).

with

$$c_m = m\prod_{n=1}^{N}\frac{\sin(m\pi\Delta\tau_n/\tau_{\max})}{m\pi\Delta\tau_n/\tau_{\max}} \tag{4b}$$

where $\tau_{\max} = \sum_{n=1}^{N}\Delta\tau_n$ and where N is the number of sections.

Hereafter, we refer to (4) as Barakat's formula. We emphasize that (4) is an exact expression for the PDF. Any errors resulting from its use are due to the numerical truncation of the Fourier series. Indeed, in all situations we tested (which included various numbers of sections between four and 22), (4) produced results equivalent to those of (3) up to roundoff error when a sufficient number of Fourier modes was used. Fig. 1 shows an extreme case in which the DGD of one section is larger than the sum of all the others. The spurious tail at small DGDs of the PDF obtained from Barakat's formula can be made arbitrarily small by using an appropriate number of Fourier modes. Note also that only values of the PDF at large DGDs are significant in the calculation of outage probabilities [7] (see also Section III), and, therefore, this tail is uninfluential except for cases in which the mean DGD is abnormally large. Note also that Barakat's formula only yields the PDF for values of DGD below $\tau_{\max}$, and above these values the PDF is taken to be automatically zero. Hence, no spurious tails are produced at large DGDs.

Most importantly, (4a) can be evaluated using the fast Fourier transform, yielding a numerical value of the PDF at a computational cost that only depends on the number of Fourier modes used and is essentially independent of the number of sections. If 2^8 Fourier modes are used, the two methods have about equal execution time for about four sections, and for 20 sections, Barakat's method has a speed advantage of about 250 000 over (3) (cf. Fig. 8 in the Appendix).

The Appendix contains a detailed comparison of the computational costs and the accuracy of the two methods. In particular, we found that 2^8 Fourier modes are sufficient to ensure that the differences in all computed values of NCR to be discussed in

Section III are comparable to the statistical error arising from the use of a finite sample of bands (e.g., 10 000 bands here and in [7]; see Appendix for further details). For this reason, we used Barakat's formula in all the numerical simulations which produced Figs. 2–8, which are discussed in Section IV.

III. Outage Probabilities and NCR

We start by discussing the computation of the outage probability for a given WDM channel following the outage map approach introduced in [10] and [11]. Recall that the two main ingredients which are needed to use this method are the outage maps and the statistical distribution of the DGD. The outage maps are plots of constant optical signal-to-noise ratio (OSNR) margins as a function of the DGD of the link and the power splitting ratio, characterizing the polarization of the input signal. The OSNR margins are allocated by the system designer to accommodate PMD impairments. Outage maps can be determined by careful simulations or measurements and depend on details of receiver design and modulation format [10]. In order to determine system outage probabilities, the outage maps are then integrated over those DGDs and signal polarizations which violate the margin specification, using the appropriate PMD statistics.

Once the PDF of the DGD has been obtained, and once a maximum OSNR penalty has been specified, the outage probability in a channel affected by first-order PMD can be written as [7]

$$P_{\text{out}}(\mathbf{z}) = \int_0^\infty p_{\text{DGD}}(\tau;\mathbf{z})\Delta\gamma(\tau)d\tau \tag{5}$$

where $0 < \Delta\gamma(\tau) < 1$ is the outage weight; that is, the fractional range of values of the splitting ratio γ that produces an outage for a given value of DGD. Note that the derivation of (5) assumes a uniform distribution γ, implying the presence of a polarization scatterer at the input of the system, with characteristics similar to those of a hinge. The required $\Delta\gamma(\tau)$ for a typical receiver was determined in [10] from numerical simulations using a 2^7 DeBrujin bit sequence, Gaussian detection statistics, a second-order Gaussian optical filter (with a 3-dB bandwidth of $2.2/T$), and a fifth-order Bessel electrical filter (with bandwidth of $0.6/T$), where T is the bit period. The OSNR penalties were simulated as a function of τ and γ for non-return-to-zero (NRZ) and 33% duty cycle return-to-zero (RZ) on-off keying (OOK) at 40 Gb/s (implying $T = 25$ ps) and at a target bit-error-ratio (BER) of 10^{-10}. The results of those numerical simulations showed that the outage weight $\Delta\gamma(\tau)$ is well-approximated by the following expression:

$$\Delta\gamma(\tau) = \sqrt{C}\sqrt{1-\left(\frac{\tau_o}{\tau}\right)^2} \tag{6}$$

for $\tau_o < \tau < \tau_1$, together with $\Delta\gamma(\tau) = 0$ for $\tau \le \tau_o$ and $\Delta\gamma(\tau) = 1$ for $\tau > \tau_1$ with

$$\tau_o = \frac{2T}{\sqrt{(A/\epsilon)+4\alpha}}, \quad \tau_1 = \frac{\tau_o}{\sqrt{1-(1/C)}} \tag{7}$$

and

$$C = 1 + \frac{4\alpha\epsilon}{A}. \tag{8}$$

Here, ϵ (in decibels) is the OSNR margin allocated to PMD, and A and α are dimensionless coefficients, which depend on the transmission format. In particular, as described in [7], $A = 51$ and $\alpha = 0.41$, for the non-return-to-zero (NRZ) format, and $A = 13$ and $\alpha = 1.04$ for a return-to-zero (RZ) format with 33% duty cycle. An immediate consequence of these relations is that if a particular concatenation of fiber sections has $\tau_{\max} < \tau_o$, the outage weight will be zero over the entire range of the DGD and, therefore, $P_{\text{out}} = 0$.

We now discuss the calculation of the NCR. In the conventional model of PMD, no statistical differences exist among channels. Thus, $p_{\text{DGD}}(\tau)$ is the same for all channels, and all channels exhibit the same outage probability. In the hinge model, however, the DGD of each section is a frozen realization from the same Maxwellian distribution. In a WDM system, channel frequencies separated by more than the PMD correlation bandwidth will, therefore, experience statistically independent values of DGD. Hence, each channel will be characterized by a different value of outage probability. In other words, P_{out} becomes itself a stochastic quantity. Recall that, to characterize the stochastic property of the system outage probabilities, the noncompliant capacity ratio (NCR) of a WDM transmission system was introduced in [7], which is defined as the expected value of the fraction of wavelength bands that have an outage probability P_{out} greater than a specified value P_{spec}

$$\text{NCR} = \mathbb{P}[P_{\text{out}}(\mathbf{z}) > P_{\text{spec}}]. \tag{9}$$

Recall also that, in the traditional model of PMD (i.e., in the case where the DGD has a Maxwellian distribution, which is equivalent to the limit of an infinite number of sections), all wavelength bands have the same outage probability P_{out}, and, therefore, the NCR is 0 for $P_{\text{spec}} > P_{\text{out}}$ and 1 for $P_{\text{spec}} < P_{\text{out}}$. As we discussed earlier, however, the outage probability in systems characterized by the hinge model can assume any value depending on the individual DGDs of the fiber sections. Then the NCR is simply the integral of the PDF of P_{out} from the specified outage P_{spec} to infinity, i.e., the complementary cumulative distribution function (CCDF) of P_{out}. That is

$$\text{NCR} = \int\int\cdots\int I[P_{\text{out}}(\mathbf{z})]p_z(\mathbf{z})\,(d\mathbf{z}), \tag{10}$$

where $(d\mathbf{z}) = dz_1\cdots dz_N$ is the volume element in $\mathbb{R}^N$, with $p_{\mathbf{z}}(\mathbf{z}) = p_{\text{Maxwell}}(z_1)\cdots p_{\text{Maxwell}}(z_N)$ being the product of N identical Maxwellian distributions, each with mean $\langle\tau\rangle$, and where $I[P_{\text{out}}]$ is an indicator function, which equals 1 if $P_{\text{out}} > P_{\text{spec}}$ and 0, otherwise.

In practice, the exact evaluation of the integral in (10) is not feasible. Here, we approximate the NCR numerically following the same procedure used in [7], but extending the computations to larger numbers of sections. Namely, we use Monte-Carlo methods to approximate the N-dimensional integral in (10). For each number of section and each value of mean DGD of the transmission span, we randomly draw a number N of section DGDs for a given wavelength band from an identical Maxwellian distribution, we evaluate the resulting PDF of the DGD, and we then integrate it over the outage map to obtain

the outage probability for that wavelength band. To obtain sufficient accuracy, we repeat the procedure for 10 000 bands as in [7] [note that, with the same personal computer used for our simulations, calculations with 10 000 wavelength bands and 20 sections would take almost three years instead of about 6 min if (3) were used instead of Barakat's formula!]. The resulting 10 000 outage probabilities are sorted, and the bands exceeding a specified outage P_{spec} are counted, yielding a numerical estimation of the NCR. Counts less than 10 are discarded to maintain good accuracy.

When smooth curves of NCR versus the mean DGD are desired (as in Figs. 4–6), the above computation needs to be repeated for about 1000 values of mean DGD. Note, however, that, once the computations have been performed for one value of mean DGD, one can obtain data at different values of mean DGD without repeating the most expensive part of the computation, which is the calculation of the PDF of the DGD. Note first that, if $\mathbf{z}_1 = (\Delta\tau_1, \ldots, \Delta\tau_N)$ collects N DGD values each distributed according to an identical Maxwellian with mean m_1, a vector $\mathbf{z}_2 = (\Delta\tau'_1, \ldots, \Delta\tau'_N)$ of N DGD values distributed according to a Maxwellian with mean m_2 is obviously obtained by simply letting $\mathbf{z}_2 = (m_2/m_1)\,\mathbf{z}_1$. But elementary scaling properties of PDFs imply that if $p_{\text{DGD}}(\tau; \mathbf{z}_1)$ is the PDF of the DGD for that realization with mean DGD m_1, the PDF for the corresponding realization with mean m_2 is $p_{\text{DGD}}(\tau; \mathbf{z}_2) = (m_1/m_2)\, p_{\text{DGD}}((m_2/m_1)\,\tau;\, \mathbf{z}_1)$.

IV. Simulations and Results

We now present the results of numerical simulations of the NCR, computed as described in Section III for both the NRZ and RZ modulation formats with various numbers of sections between four and 20. In all these simulations, we used 2^8 Fourier modes and 10 000 wavelength bands and we set the OSNR margin ϵ to 1 dB.

Figs. 2–6 show in detail the results obtained for transmission links with ten and 20 sections. These are, for $N = 10$ and $N = 20$, exactly the same kinds of figures as those that were given in [7] for the case of $N = 6$. Indeed, even though to avoid duplication we omit the figures for $N = 6$ here (with the exception of Fig. 3(a), which shows the NCR versus P_{spec} for RZ systems with $N = 6$ sections which was not shown in [7]), the present figures are intended to complement those in [7], and we emphasize that the reader should compare Figs. 2–6 here to [7, Figs. 2–4] in order to fully appreciate the result of increasing the number of sections.

Fig. 2 shows the NCR as a function of P_{spec} for systems with $N = 10$ and $N = 20$ sections using the NRZ modulation format, while Fig. 3 does the same for systems using the RZ modulation format. As already demonstrated in [7], the NCR undergoes a gradual transition from the value 0 (obtained for $P_{\text{spec}} = 1$) to its asymptotic value in the limit $P_{\text{spec}} \to 0$, which is well approximated by

$$\text{NCR}_{0,\text{approx}} = \frac{1}{2}\,\text{erfc}\left(\frac{(\tau_o/\langle\tau\rangle) - \sqrt{N}}{\sqrt{(3\pi/4) - 2}}\right). \qquad (11)$$

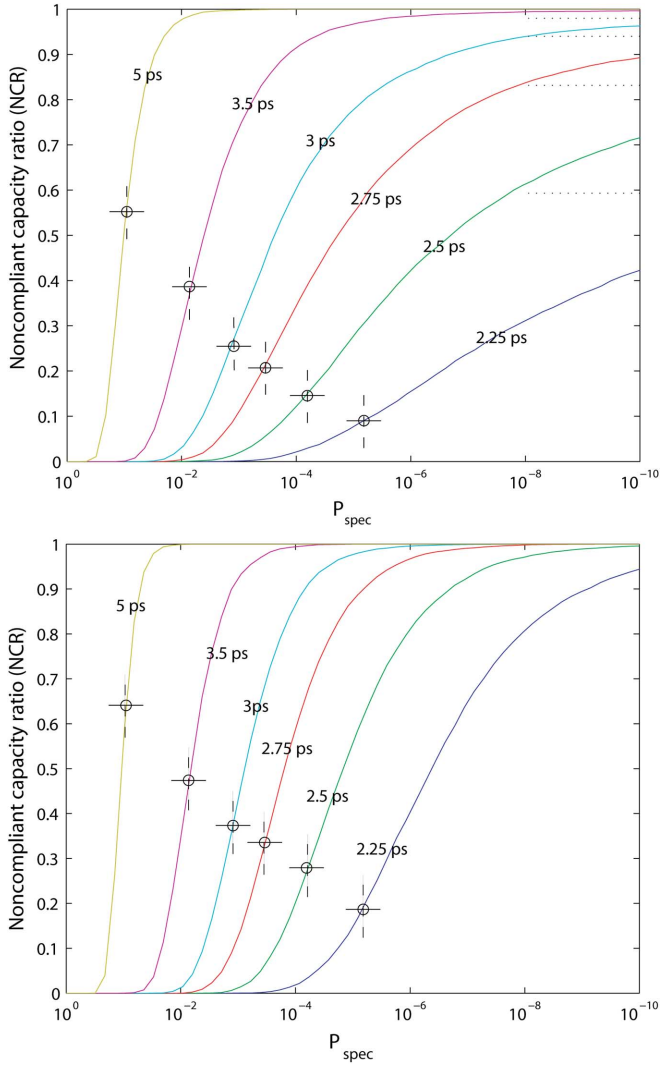

Fig. 2. NCR as a function of P_{spec} with 40-Gb/s NRZ modulation. Top: Plot for links of ten sections. Bottom: Plot for links of 20 sections. The link's mean DGD is indicated on each curve. The dashed lines indicate the traditional outage probabilities, computed using (12). The dotted horizontal lines are the asymptotes of zero outage probability for each mean DGD, computed using (11).

Comparing Fig. 3 with [7, Fig. 2] for the case $N = 6$, one sees how the curves become progressively steeper, tending to their asymptotic limit as $N \to \infty$.

Fig. 4 shows the mean DGD versus the outage probability for fixed values of NCR, again for $N = 10$ and $N = 20$, and for both NRZ and RZ. The traditional outage curves are calculated using the following formula:

$$P_{\text{out}} = \sqrt{1 + \frac{4\alpha\epsilon}{A}}\,\exp\left[-\frac{16\epsilon T^2}{\pi(A + 4\alpha\epsilon)\langle\tau\rangle^2}\right] \qquad (12)$$

where, again, $\langle\tau\rangle$ is the mean DGD of the line (the corresponding formula used in [7] contains an error, corrected in [13]).

Again, one should compare these curves to the curves in the case $N = 6$, which were given in [7, Fig. 3].

Finally, Figs. 5 and 6 show the NCR as a function of normalized mean DGD for several different outage specifications. The

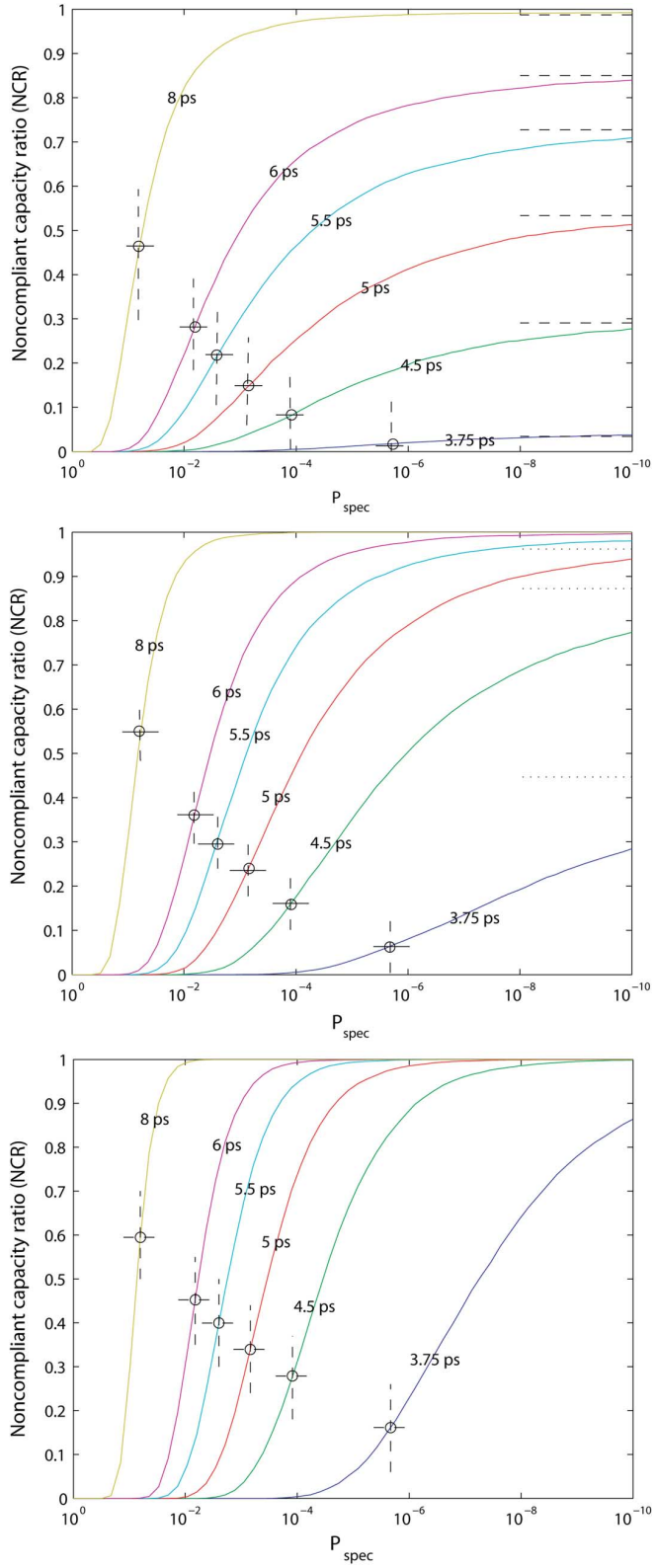

Fig. 3. Same as Fig. 2, but for the RZ transmission format. Top: $N = 6$ (which was not shown in [7]). Middle: $N = 10$. Bottom: $N = 20$.

limit of zero outage is shown as a dot-dashed curve. Comparing these results to those for $N = 6$, which were given in Fig. 4 of [7], one notices once more how the curves become progressively steeper as N increases.

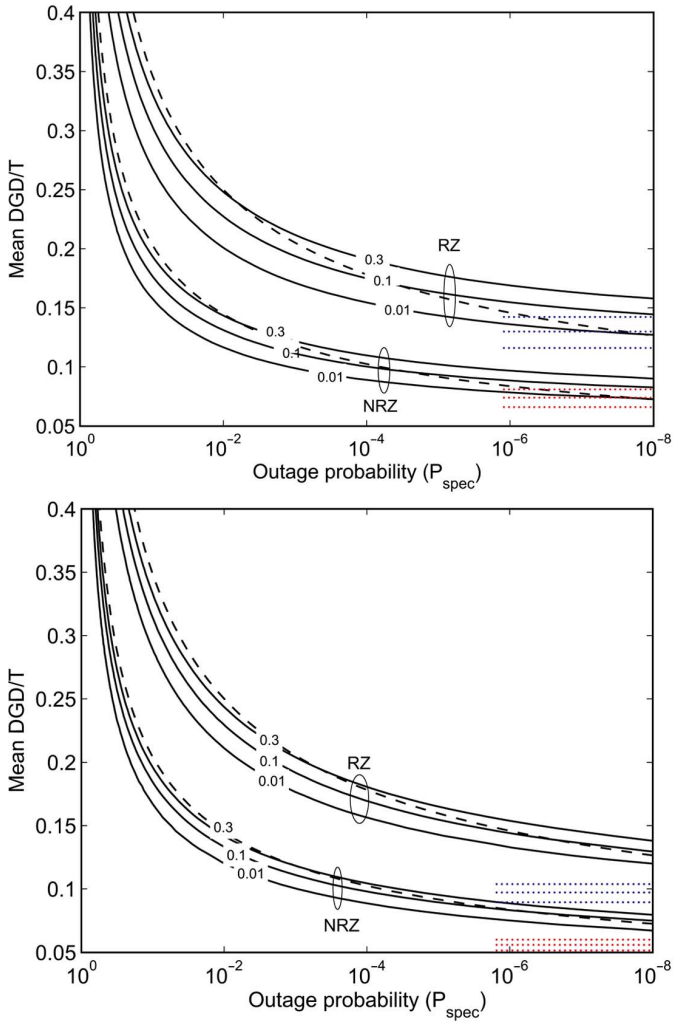

Fig. 4. Mean DGD$/T$ of the link required for specified outage probability. Top: Links of ten sections. Bottom: Links of 20 sections. Contours for $\mathrm{NCR} = 0.01, 0.1, 0.3$ are shown. The traditional outage curves, obtained from (12), are shown as dashed lines. The dotted lines show the corresponding asymptotic values of mean DGD in the limit of zero outage probability for the RZ and the NRZ formats, as obtained from (11).

Fig. 7 summarizes the above results by showing explicitly the dependence of the NCR on the number of sections N for systems with two different values of P_{spec}, for both the NRZ and the RZ modulation formats. The increased robustness of the RZ format to PMD, compared to the NRZ format, is once more evident from these data.

V. Conclusion

We have presented a method for the computation of precise outage specifications for transmission spans characterized by the hinge model of PMD for varying numbers of sections. The method uses the simulated outage maps and an expression for the PDF of the DGD originally obtained by Barakat. We then applied the method to study systems with $N = 10$ and $N = 20$ sections. The resulting figures complement those for $N = 6$ in [7]. In particular, the curves in Figs. 2–6 show significant steepening as the section number increases. Note, however, that, even for 20 sections, significant differences remain as compared to

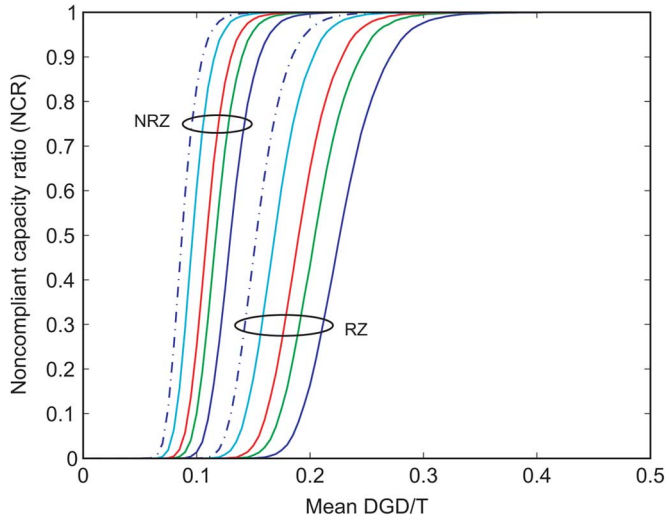

Fig. 5. NCR versus mean DGD/T for systems with ten sections and with specified values of the outage probability. The outage probabilities associated to each curve are, from left to right, 10^{-8}, 10^{-5}, 10^{-4}, and 10^{-3}, respectively. The limiting value of the NCR for zero outage is shown in the dot-dashed curves.

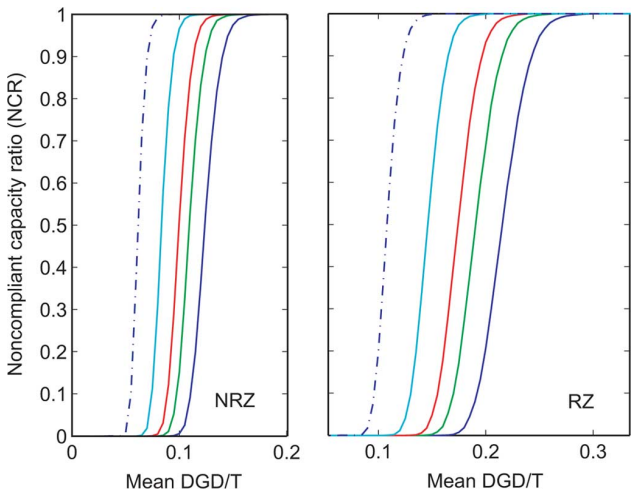

Fig. 6. Same as Fig. 5, but for systems with 20 sections. Left: NRZ format. Right: RZ format.

the step function which is characteristic of the outage behavior in the traditional model of PMD.

APPENDIX

Here, we compare the relative speed and accuracy of the two methods for the computation of the PDF of the DGD discussed in Section II, namely Antonelli and Mecozzi's (A&M's) formula (3) and Barakat's sine series (4).

We first compare the computational cost of the two methods of evaluating the PDF of the DGD discussed in Section II. Fig. 8 shows the execution time for various numbers of sections with the two methods, both optimized for speed to the best of our ability. The two methods have about equal execution time for about four sections if $N_f = 2^8$ Fourier modes are used, or seven sections with $N_f = 2^{11}$ modes. For a larger number of sections, the time required to evaluate (3) increases by a factor of two for every added section, as expected, while the time required to compute (4) stays about constant. For 20 sections, the latter has a speed advantage of about 250 000 when 2^8 Fourier

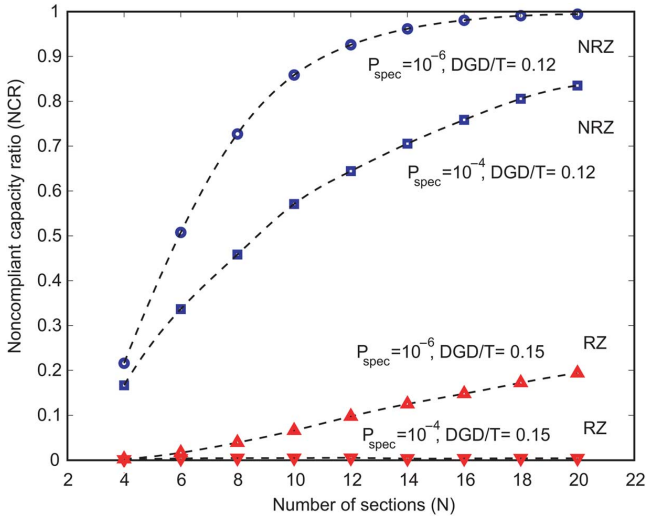

Fig. 7. NCR as a function of the number of sections N of RZ and NRZ systems with various mean DGDs and outage specifications. Circles: NRZ with $P_{\text{spec}} = 10^{-6}$ and mean DGD$/T = 0.12$; squares: NRZ with $P_{\text{spec}} = 10^{-4}$ and mean DGD$/T = 0.12$; upward triangles: RZ with $P_{\text{spec}} = 10^{-6}$ and mean DGD$/T = 0.15$; downward triangles: RZ with $P_{\text{spec}} = 10^{-4}$ and mean DGD$/T = 0.15$.

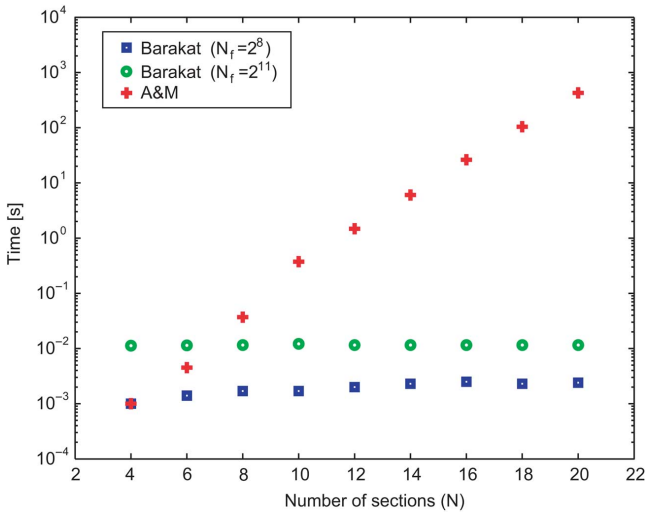

Fig. 8. Time (in seconds) required to calculate the PDF of DGD using, respectively, Barakat's formula (4) with 2^8 and 2^{11} Fourier modes and the formula in [9], as a function of the number of sections N. The calculations were performed on a 2.40-GHz Pentium 4 personal computer using Matlab version 7.0 (R14).

modes are used. It should be noted that, as mentioned in [9], at most, half of the 2^N terms in (3) are nonzero, and, therefore, (3) could be computed by evaluating 2^{N-1} terms instead of 2^N. To take advantage of this fact, however, one must identify all the nonzero combinations beforehand, index them, and then recall them every time the PDF must be evaluated. In theory, this could save a factor 2 in speed (in practice, the actual saving might be smaller depending on how much overhead is needed for the indexing). For simplicity, our code simply evaluates all 2^N combinations. However, even a speedup of (3) by a factor of 2 would not alter significantly the speed comparison.

We now discuss the relative accuracy of the two methods. It would be fairly easy to plot the PDF of the DGD with both methods and compute the relative difference. Rather than doing so, however, we believe that it is more appropriate to study how

TABLE I
ERROR COMPARISONS FOR THE CALCULATION OF THE NCR

	$N_{MC} = 10,000$		$N_{MC} = 40,000$	
DGD	2.25 ps	5 ps	2.25 ps	5 ps
A	0.0014	0.0047	0.0017	0.0037
B_4	0.0038	0.0117	0.0016	0.0065
B_6	0.0059	0.0090	0.0018	0.0034
B_8	0.0072	0.0126	0.0058	0.009
B_{10}	0.0018	0.0119	0.0041	0.0086
C_4	0.03	0.022	0.0383	0.0118
C_6	0.0047	0.0048	0.0071	0.0039
C_8	0.0042	0.0090	0.0026	0.0115
C_{10}	0.0050	0.0085	0.0020	0.0052

any errors in the determination of the PDF reflect in the calculation of the NCR, since the NCR is ultimately the quantity of interest. Thus, Table I shows the differences between the values of the NCR as obtained from the following comparisons.

- A — A&M twice.
- B_4 — Barakat twice with $N_f = 2^4$.
- B_6 — Barakat twice with $N_f = 2^6$.
- B_8 — Barakat twice with $N_f = 2^8$.
- B_{10} — Barakat twice with $N_f = 2^{10}$.
- C_4 — A&M versus Barakat with $N_f = 2^4$.
- C_6 — A&M versus Barakat with $N_f = 2^6$.
- C_8: — A&M versus Barakat with $N_f = 2^8$.
- C_{10} — A&M versus Barakat with $N_f = 2^{10}$.

That is, case A compares the values of the NCR obtained running the simulations twice (that is, with two different random samples of wavelength bands) using in both cases Antonelli and Mecozzi's formula (3). Cases B_4–B_{10} compare the values obtained using Barakat's formula with two different random samples of wavelength bands, using either $N_f = 2^4(B_4), N_f = 2^6(B_8)$, $N_f = 2^8(B_8)$ or $N_f = 2^{10}(B_{10})$ Fourier modes. Finally, cases C_4 to C_{10} compare the results obtained using A&M's formula versus those obtained using Barakat's formula (4a), again with $N_f = 2^4(C_4), N_f = 2^6(C_6)$, $N_f = 2^8(C_8)$ or $N_f = 2^{10}(C_{10})$ Fourier modes. In all these cases, the comparisons were done for an NRZ system with 6 sections and for two different values of mean DGD: 2.25 and 5 ps, and with sample sizes of either $N_{MC} = 10\,000$ or $N_{MC} = 40\,000$ wavelength bands. In each of these cases, the value in the table is the maximum difference in the values of the NCR obtained with the two methods, taken across the whole range of values of P_{spec}.

To interpret these numbers, it is important to realize that there are two sources of errors in the calculation of the NCR: i) the statistical error due to the use of finite number of wavelength bands; and, if Barakat's formula is used, ii) the truncation error due to the use of finite number of Fourier modes (we assume that roundoff error is negligible here). The computation of the NCR using A&M's formula is not affected by truncation error, but it is affected by statistical error. Thus, the differences among the values of the NCR reported in the first row of Table I are an indication of the size of the pure statistical error resulting from the use of a given number of wavelength bands. More precisely, the differences reported are an estimate of the standard deviation of the result, obtained by making only two measurements. Note, however, that the values in Table I are, of course, themselves affected by statistical fluctuations and are, thus, not a precise measure of the error.

Based on the above considerations, the values in Table I then suggest the following conclusions. First, the error due to finite truncation of the Fourier series when 2^8 or more Fourier modes are used is of the same order of magnitude as the pure statistical error. Second, increasing the number of Fourier modes from 2^8 to 2^{10} does not seem to reduce the total error significantly in most cases. We, therefore, conclude that the use of 2^8 Fourier modes is adequate when 10 000 samples of wavelength bands are used. Of course, if more precise results are desired, one must increase the number of Fourier modes *as well as* the number of wavelength bands. Finally, note that, even when the absolute error is small, the relative error incurred can be large for small values of the NCR, even when A&M's method is used. This is because, if NCR is small, a very small fraction of wavelength bands are noncompliant, and, therefore, calculating the NCR via Monte Carlo methods suffers from the usual problems of rare event estimation.

ACKNOWLEDGMENT

The authors would like to thank M. Boroditsky, M. Brodsky, W. L. Kath, and L. E. Nelson for many valuable discussions.

REFERENCES

[1] C. D. Poole and J. A. Nagel, "Polarization effects in lightwave systems," in *Optical Fiber Telecom. IIIA*, I. P. Kaminow and T. L. Koch, Eds. San Diego, CA: Academic, 1997.
[2] H. Kogelnik, L. E. Nelson, and R. M. Jopson, "Polarization mode dispersion," in *Optical Fiber Telecommunications IVB*, I. P. Kaminow and T. Li, Eds. San Diego, CA: Academic, 2002, pp. 725–861.
[3] Boroditsky, P. Magill, N. J. Frigo, and M. Tur, "Channel-to-channel variation of non-Maxwellian statistics of DGD in a field installed system," in *Proc. ECOC*, 2004, vol. 3, pp. 306–309.
[4] M. Boroditsky, M. Brodsky, P. Magill, N. J. Frigo, C. Antonelli, and A. Mecozzi, "Outage probabilities for fiber routes with finite number of degree of freedom," *IEEE Photon. Technol. Lett.*, vol. 17, no. 2, pp. 345–347, Feb. 2005.
[5] M. Brodsky, N. J. Frigo, M. Boroditsky, and M. Tur, "Polarization mode dispersion of installed fibers," *IEEE J. Lightw. Technol.*, vol. 24, no. 12, pp. 4584–4599, Dec. 2006.
[6] C. Antonelli and A. Mecozzi, "Theoretical characterization and system impact of the hinge model of PMD," *IEEE J. Lightw. Technol.*, vol. 24, no. 12, pp. 4064–4074, Dec. 2006.
[7] H. Kogelnik, P. Winzer, L. E. Nelson, R. M. Jopson, M. Boroditsky, and M. Brodsky, "First-order PMD outage for the hinge model," *IEEE Photon. Technol. Lett.*, vol. 17, no. 6, pp. 1208–1210, Jun. 2005.
[8] R. Barakat, "Isotropic random flights," *J. Phys. A: Math., Nucl. Gen.*, vol. 6, pp. 796–804, Jun. 1973.
[9] C. Antonelli and A. Mecozzi, "Statistics of the DGD in PMD emulators," *IEEE Photon. Technol. Lett.*, vol. 16, no. 8, pp. 1804–1806, Aug. 2004.
[10] P. J. Winzer, H. Kogelnik, and K. Ramanan, "Precise outage specifications for first-order PMD," *IEEE Photon. Technol. Lett.*, vol. 16, no. 2, pp. 449–451, Feb. 2004.
[11] H. Bulow, "Operation of digital optical transmission system with minimal degradation due to polarisation mode dispersion," *Electron. Lett.*, vol. 31, pp. 214–215, 1995.
[12] J. P. Gordon and H. Kogelnik, "PMD fundamentals: Polarization-mode dispersion in optical fibers," *Proc. Nat. Acad. Sci.*, vol. 97, pp. 4541–4550, Apr. 2000.
[13] P. J. Winzer and H. Kogelnik, "Corrections to "Receiver impact on first-order PMD outage"," *IEEE Photon. Technol. Lett.*, vol. 30, no. 3, p. 458, Mar. 2008.

Jinglai Li was born on December 5, 1979, in Binzhou, China. He received the B.S. degree in applied mathematics from Sun Yat-sen University, Guangzhou, China, in 2002, and the M.A. degree in mathematics and the Ph.D. degree in applied mathematics from the State University of New York at Buffalo in 2004 and 2007, respectively.

Since 2007, he has been a Postdoctoral Fellow with the Department of Engineering Sciences and Applied Mathematics, Northwestern University, Evanston, IL. His research interests include optical solitons, fiber-optic communications, and ultrafast lasers.

He is a member of the American Mathematical Society and the Society for Industrial and Applied Mathematics.

Gino Biondini was born November 18, 1966, in Perugia, Italy. He received the Laurea degree in physics and the Doctorate degree in theoretical physics from the University of Perugia in 1991 and 1997, respectively.

From 1997 to 1999, he was a Postdoctoral Research Associate at the University of Colorado, Boulder; from 1999 to 2001, he was a Research Assistant Professor at Northwestern University, Evanston, IL; and from 2001 to 2004, he was a Zassenhaus Assistant Professor at The Ohio State University, Columbus. In Fall 2004, he joined the Department of Mathematics, State University of New York at Buffalo, where he is now an Associate Professor.

His research interests include analytical and computational methods for nonlinear optics and optical fiber communications, nonlinear wave equations, solitons and integrable systems, applied probability and stochastic processes, and variance reduction techniques. He has authored more than 40 refereed journal publication and holds two U.S. patents about applications of importance sampling to polarization-induced effects.

Herwig Kogelnik (M'61–F'73–LF'98) was born in Graz, Austria, in 1932. He received the Dipl. Ing. and Dr. Tech. degrees in electrical engineering from the Technical University of Vienna, Austria, in 1955 and 1958, respectively, and the D.Phil. degree in physics from Oxford University, Oxford, U.K., in 1960.

In 1961, he joined the research division of Bell Labs (now Alcatel-Lucent), Holmdel, NJ, and is currently the Adjunct Photonics Systems Research Vice President.

Dr. Kogelnik is currently a Fellow and past President (1989) of the Optical Society of America (OSA), as well as a Member of the National Academy of Science and the National Academy of Engineering. He is an Honorary Fellow of St. Peters College, Oxford.

Peter J. Winzer (SM'06) received the M.S. and Ph.D. degrees in electrical/communications engineering from the Vienna University of Technology, Vienna, Austria, in 1996 and 1998, respectively.

His academic work, which was largely supported by the European Space Agency, was related to the analysis and modeling of spaceborne Doppler wind lidar and highly sensitive free-space optical communication systems. In this context, he specialized in optical modulation formats and high-sensitivity receivers using coherent and direct detection. He continued to pursue this field of research after joining Bell Laboratories, Lucent Technologies, Holmdel, NJ, in 2000, where he focused on Raman amplification, optical modulation formats, advanced receiver concepts, and digital signal processing and advanced modulation for 10-, 40-, and 100-Gb/s fiber-optic communication systems. More recently, he has been working on higher layer data networking problems. He has authored or coauthored more than 100 papers published in international journals and conference proceedings, as well as five book chapters. He is the holder of several patents in the aforementioned fields.

Dr. Winzer is a member of the Optical Society of America.